1H NMR Investigation of the Paramagnetic Cluster Environment in Pyrococcus furiosus Three-Iron Ferredoxin: Sequence-Specific Assignment of Ligated Cysteines Independent of Tertiary...

7 AUTHORS, INCLUDING:

Quincy Teng
United States Environmental Protection Age…
79 PUBLICATIONS **1,992** CITATIONS

SEE PROFILE

Luigi Calzolai
European Commission
49 PUBLICATIONS **1,963** CITATIONS

SEE PROFILE

¹H NMR Investigation of the Paramagnetic Cluster Environment in *Pyrococcus furiosus* Three-Iron Ferredoxin: Sequence-Specific Assignment of Ligated Cysteines Independent of Tertiary Structure[†]

Carol M. Gorst,[‡] You-Hsing Yeh,[‡] Quincy Teng,[‡,§] Luigi Calzolai,[‡,‖] Zhi-H. Zhou,[⊥] Michael W. W. Adams,[⊥] and Gerd N. La Mar*,[‡]

Department of Chemistry, University of California, Davis, California 95616 and Department of Biochemistry, University of Georgia, Athens, Georgia 30602

Received August 26, 1994; Revised Manuscript Received November 4, 1994[®]

ABSTRACT: One- and two-dimensional ¹H NMR data tailored to detect paramagnetically relaxed protons near the $S = \frac{1}{2}$, three-iron−sulfur cluster of the ferredoxin from the hyperthermophile *Pyrococcus furiosus* are analyzed to sequence specifically assign the hyperfine shifted ligated cysteine signals, to determine the nature of the secondary structural elements on which these cysteines reside, and to define the tertiary contacts of the cluster with the remainder of the previously characterized secondary structure remote from the cluster [Teng, Q., Zhou, Z.-H., Busse, S. C., Howard, J. B., Adams, M. W. W., & La Mar, G. N. (1994) *Biochemistry 33*, 6316−6326]. Inspection of the geometry of the cluster ligating cysteines in the six structurally characterized cubane ferredoxin (Fd) clusters reveals a pattern of distances from the cluster iron(s) that indicate that each Cys will exhibit one backbone proton that will allow the detection of dipolar connectivities to the backbone of adjacent residues. It is expected that the first and last of the Cys in the cluster consensus binding sequence will exhibit weakly relaxed peptide NH and strongly relaxed $C_{\alpha}H$ signals, while the two central Cys in that sequence will exhibit strongly relaxed peptide NH but weakly relaxed $C_{\alpha}H$ peaks. These dipolar contacts are clearly observed for the three ligated Cys in 3Fe *P. furiosus* Fd, providing the first sequence specific assignment of ligated cysteines which do not explicitly require knowledge of the tertiary structure of the protein. This approach is proposed to have very general application to cubane ferredoxins. A combination of steady-state NOEs and short mixing time NOESY experiments demonstrate that Cys¹⁷ is on a short helix through Leu²⁰ and that Cys⁵⁶ likely initiates a type I turn, as observed in the crystal structure of the 3Fe Fd for *Desulfovibrio gigas* [Kissinger, C. R., Sieker, L. C., Adman, E. T., & Jensen, L. H. (1991) *J. Mol. Biol. 219*, 693−715]. The observed relaxation rates of resolved or partially resolved signals are shown to correlate with their proximity to the various iron in the cluster, as determined for the homologous residues in *D. gigas* Fd, providing additional qualitative information on tertiary contacts of the cluster.

Ferredoxins (Fds)[1] are small electron transfer proteins that contain one or two iron−sulfur clusters as redox center(s). The cluster architectures fall into two main classes, the two-iron or plant-type Fd which exhibit only localized valence (i.e., $2Fe^{3+}$ for $[Fe_2S_2]^{2+}$ in Fd^{ox} and $1Fe^{3+};1Fe^{2+}$ for $[Fe_2S_2]^{1+}$ in Fd^{red}), and the cubane or bacterial-type Fd which

exhibit valence delocalization over pairs of iron in both their four-iron (i.e., $4Fe^{2.5+}$ in $[Fe_4S_4]^{2+}$ for Fd^{ox}, $2Fe^{2.5+}$; $2Fe^{2+}$ in $[Fe_4S_4]^{1+}$ for Fd^{red}) and three-iron ($3Fe^{3+}$ in $[Fe_3S_4]^{1+}$ for Fd^{ox}, $2Fe^{2.5+};1Fe^{3+}$ in $[Fe_3S_4]^0$ for Fd^{red}) forms (Cammack et al., 1977; Thompson, 1985; Beinert, 1990; Howard & Rees, 1991; Cammack, 1992; Münck et al., 1988). A schematic structure of a cubane cluster is illustrated in Figure 1. The related, but more oxidizing cubane cluster of high-potential iron−sulfur proteins, Hipip, exhibit the same ground state for $Hipip^{red}$ as $4Fe Fd^{ox}$, but with $2Fe^{2.5+}$; $2Fe^{3+}$ in $[Fe_4S_4]^{3+}$ for $Hipip^{ox}$ (Cammack et al., 1977). The cluster environment therefore is modulated strongly by the protein matrix not only to vary the overall cluster redox potential but also to differentiate the redox properties of individual or pairs of iron atoms within the cluster. While the tendency for the cubane clusters to exhibit asymmetry appears to be an intrinsic property of even the symmetrical model compounds (Holm, 1977; Bominaar et al., 1994), this distortion is "locked in" by the asymmetric protein matrix in a fashion likely dictated by the need to control the flow of electrons (Langen et al., 1992). The mechanism by which the cluster environment modulates the location of the reducing electron may become clear when both the detailed molecular structure

---

* Address correspondence to this author.

[‡] Department of Chemistry, University of California, Davis, CA 95616.

[§] Present address: Department of Chemistry, University of Georgia, Athens, GA 30602.

[‖] Present address: Department of Chemistry, University of Siena, Siena, Italy.

[⊥] Department of Biochemistry, University of Georgia, Athens, GA 30602.

[1] Abbreviations: Fd, ferredoxin; Hipip, high-potential iron−sulfur protein; Pf, *Pyrococcus furiosus*; Dg, *Desulfovibrio gigas*; Pa, *Peptococcus aerogenes*; Bt, *Bacillus thermoproteolyticus*; Av, *Azotobacter vinlandii*; Cp, *Clostridium pasteurianum*; Cau, *Clostridium acidi urici*; DSS, 2,2′-dimethyl-2-silapentane-5-sulfonate; ppm, parts per million; NOE, nuclear Overhauser effect; NOESY, 2D nuclear Overhauser spectroscopy; TOCSY, 2D total correlation spectroscopy; NMR, nuclear magnetic resonance.
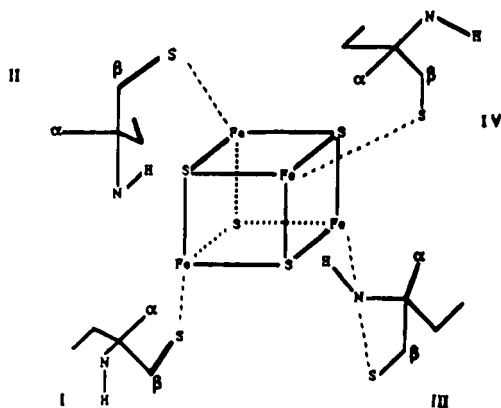
FIGURE 1: Schematic structure of the iron—sulfur cluster of a bacterial ferredoxin with the ligating Cys I—IV, as found[2] in *Pa*, *Av*, *Dg*, and *Bt* Fd. The orientations of the four Cys, with $C_\alpha H$ of Cys I, IV and $N_P H$ of Cys II, III oriented toward the cluster, and $C_\alpha H$ for Cys II, III and $N_P H$ for Cys I, IV oriented away from the cluster iron, is common[4] to those Fd even when one ligating Cys (Cys II) is absent in the Fe_3S_4 cluster of *Dg* and *Av* Fd.

and sequence identification of the individual iron become available for a variety of iron—sulfur proteins.

The strong magnetic coupling in all oxidation states of 2Fe, 3Fe, and 4Fe Fd results in spin magnetization with a temperature dependence that is highly characteristic of the valence state for individual iron atoms in a cluster. This spin magnetization for each iron, in turn, is reflected in the contact shift for the resonances of the ligated cysteine. Thus the larger spin vectors for the one Fe^{3+} in 2Fe Fd^{red}, and the valence-delocalized pair $2Fe^{2.5+}$ in 4Fe Fd^{red} or 3Fe Fd^{red}, are aligned parallel with the applied field at all temperatures and hence will exhibit Curie-like temperature dependence. In contrast, the smaller spin vectors for the Fe^{2+} in 2Fe Fd^{red}, the Fe^{3+} in 3Fe Fd^{red}, or the pair $2Fe^{2+}$ in 4Fe Fd^{red} are aligned against the field at low temperature and therefore will exhibit anti-Curie temperature dependence (Phillips & Poe, 1973; Dunham et al., 1971; Banci et al., 1990; Bertini et al., 1991, 1992a; Luchinat & Ciurli, 1993). The identification of which pair of Cys determine the location of the added electron in either 3Fe or 4Fe Fd^{red} is uniquely addressable by ¹H NMR spectroscopy if the broadened and contact shifted Cys $C_\beta H$ resonances can be sequence-specifically assigned. To date, all sequence-specific assignments of the contact shifted Cys resonances in an iron—sulfur protein have relied on observing inter-Cys or Cys—protein tertiary contacts predicted from the known molecular structure of the same or a homologous protein (Dugad et al., 1990; Skjeldal et al., 1991; Bertini et al., 1992b, 1993, 1994; Banci et al., 1993; Nettesheim et al., 1992; Macedo et al., 1993b; Donaire et al., 1994; Chae et al., 1994a).

The molecular structure of several Fds containing 2Fe, 3Fe, and 4Fe clusters have been determined by X-ray crystallography [see, for example, Table III in Cammack et al. (1992)]. Modern 2D NMR methods, in general, can also provide the molecular structure of such small proteins (Wüthrich, 1986), and extensive but incomplete assignments have been reported for a variety of Fd and Hipip (Nettesheim et al., 1992; Gaillard et al., 1992, 1993; Banci et al., 1993; Bertini et al., 1992b, 1993, 1994; Teng et al., 1994; Oh & Markley, 1990; Ye et al., 1992; Chae et al., 1994b). However, the same cluster paramagnetism which induces the valuable Cys contact shifts that are diagnostic of the iron

valence-state also leads to relaxation which interferes with the efficacy of the standard 2D experiments (La Mar & de Ropp, 1993) and hence to loss of information for residues near the cluster. 2D NMR studies on iron—sulfur cluster proteins have yielded incomplete information on the portion of the protein near the active site that ranges from 8 Å from the cluster in 2Fe Fd (Oh & Markley, 1990; Ye et al., 1992; Chae et al., 1994a,b) to ~5 Å from the cluster in 3Fe, 4Fe Fd, or Hipip (Nettesheim et al., 1992; Gaillard et al., 1992, 1993; Bertini et al., 1994; Teng et al., 1994). One approach for expanding the information base near the cluster is to rely on heteronuclear NMR of labeled proteins, for which relaxation effects at comparable distances to the cluster are significantly smaller than for protons because of the γ^2 dependence (Oh & Markley, 1990; Chae et al., 1994a,b). However, isotope-labeling of many interesting Fd is not yet practical. Optimally, both ¹H homonuclear and heteronuclear NMR methods need to be further developed.

We are interested in the electronic (magnetic) and molecular structural properties of the ferredoxins from a number of hyperthermophilic archae, such as *Pyrococcus furiosus* (*Pf*) and *Thermococcus litoralis* (*Tl*), which grow optimally near 100 °C in deep sulfide-rich marine environments (Fiala & Sletter, 1986; Neuner et al., 1990). In addition to the interest in the cluster electronic structure, these Fds are candidates for detailed molecular structure determination to elucidate the structural basis for their remarkable thermo-stability. To date, however, these Fd have failed to yield suitable single crystals, and hence a solution ¹H NMR study has been initiated on 3Fe *Pf* Fd (Busse et al., 1992; Teng et al., 1994). The sequence for *Pf* Fd is compared in Figure 2 with that of the Fd from *Desulfovibrio gigas* (*Dg*) using the common labeling I—IV for the consensus sequence ligand positions. A high-resolution X-ray crystal structure of the 3Fe form of *Dg* Fd has been reported for which Cys^{11} (or Cys II) is not ligated (Kissinger et al., 1991); the other two Cys, labeled V and VI in Figure 2B, form a disulfide bridge. One of the four Cys in the *Pf* Fd consensus sequence for the cluster (position II) is substituted (i.e., Asp^{14}), which allows facile removal of one Fe from the functional protein to yield a 3Fe Fd. The asymmetric coupling of the three Fe^{3+} in the $S = 1/2$ ground state (Connover et al., 1990) results in a pattern of contact shifts with one Cys exhibiting Curie-like, and two Cys exhibiting anti-Curie temperature behavior (Busse et al., 1992) similar to that observed for Dg 3Fe Fd (Macedo et al., 1993a). The asymmetry may be related to the asymmetry in the reduced cluster with $S = 2$, arising from $2Fe^{2.5+};1Fe^{3+}$, where the reducing electron is also valence delocalized over a particular pair of iron atoms (Münck et al., 1988).

The molecular/electronic structure of 3Fe *Pf* Fd has been addressed in two previous reports which have dealt with essentially nonoverlapping portions of the protein. On the one hand, the rapidly relaxed ($T_1 \sim 2-10$ ms) and contact shifted signals have been located and assigned non-sequence-specifically to the three ligated Cys, and the asymmetric—magnetic coupling has been characterized (Busse et al., 1992). On the other hand, the solution secondary structure of 3Fe Fd^{ox} was investigated by standard 2D NMR methods which assigned a majority of the residues remote from the cluster and showed that the overall folding topology is similar to that of *Dg* Fd in many respects (Teng et al., 1994). There were also observed important differences, such as expansion
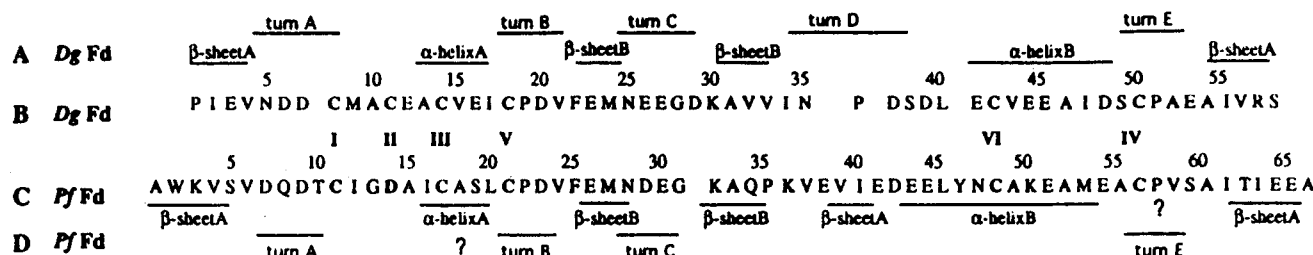
		turn A			turn B	turn C		turn D			turn E	
A *Dg* **Fd**	β-sheetA		α-helixA	β-sheetB	β-sheetB		α-helixB	β-sheetA

```
                    5        10        15       20       25       30       35          40        45      50       55
B   Dg Fd       P I E V N D D  C M A C E A C V E I  C P D V F E M N E E G D K A V V  I N    P   D S D L   E C V E E  A I D S C P A E A  I V R S
```

```
                       I     II   III        V                                              VI           IV
                   5       10        15       20       25       30           35      40      45      50      55      60      65
C   Pf Fd       A W K V S V D Q D T C  I G D A  I C A S L C P D V F E M N D E G   K A Q P  K V E V  I E D E E L Y N C A K E A M E A C P V S A  I T I E E A
```

D *Pf* **Fd**	β-sheetA		α-helixA		β-sheetB	β-sheetB	β-sheetA	α-helixB		?	β-sheetA
	turn A		?	turn B	turn C				turn E		

FIGURE 2: Amino acid sequence of *Pf* Fd (C) compared with that of *Dg* Fd (B). The alignment is made on the basis of the Cys I−VI, of which Cys I, III, and IV ligate the cluster and Cys V and VI participate in a disulfide bridge. Cys II is not ligated in *Dg* 3Fe Fd and is replaced by a nonligated Asp^{14} in *Pf* 3Fe Fd. The secondary structure elements identified in the crystal structure of *Dg* 3Fe Fd (Kissinger et al., 1991) are shown in A, while the same elements deduced from solution ^1H NMR (Teng et al., 1994) are shown in D.

of a double- to a triple-stranded β-sheet and extension and translation toward the C-terminus of a key helix. The comparison of the available secondary structural elements between *Dg* and *Pf* Fd is shown in Figure 2. The standard 2D methods, however, did not provide the necessary NMR data to ascertain whether the small helix (labeled A? in Figure 2D) and the β-turn after ligand Cys^{56}(IV) (labeled turn E? in Figure 2D) are retained in *Pf* relative to *Dg* Fd.

In this report we explore the use of 1D and 2D NMR methods that emphasize efficiently relaxed protons (La Mar & de Ropp, 1993) to sequence-specifically identify the ligated Cys in a manner that does not rely on tertiary structure (i.e., via the standard $C_αH$, NH backbone connections) (Wüthrich, 1986). These assigned Cys signals are then used to further investigate the secondary structural elements on which the ligated Cys are positioned. Lastly, we will explore the prospects for defining the position of the cluster (i.e., tertiary contacts) relative to the remainder of the protein structure described previously. The long-term goal is to develop both conventional (2D) and unconventional (steady-state NOE, paramagnetic relaxation) structural constraints that will assist in developing a robust molecular model for paramagnetic Fds based on NMR data.

MATERIALS AND METHODS

Proteins. *Pyrococcus furiosus* (*Pf*) (DSM 3638) was grown and its ferredoxin was purified under strict anaerobic conditions as described previously (Aono et al., 1989). The ferredoxin was converted to the 3Fe form with excess ferricyanide (Conover et al., 1990). NMR samples were prepared by exchanging the ^1H_2O solution with a 50 mM sodium phosphate buffer, pH 7.8, in ^1H_2O or ^2H_2O where indicated, using an Amicon ultrafiltration device. 2D NMR samples were 8 mM in protein.

NMR Spectroscopy. All ^1H NMR spectra were recorded at 500 MHz on a GE Omega 500 spectrometer. Chemical shift values were referenced to 2,2-dimethyl-2-sulfonate, DSS, through the residual solvent signal at 4.71 ppm at 30 °C and 4.61 ppm at 40 °C. Spectra were collected by the normal one-pulse sequence with ^1H_2O presaturation using a slow recycle time (3 s) or with the super-WEFT pulse sequence (Inubishi et al., 1983) utilizing a faster recycle time (~180 ms). Nonselective spin−lattice relaxation times were collected with an inversion−recovery pulse sequence; recycle times were set at ~5 times the T_1 times for the peaks of interest. T_1 values were determined from the initial slope of the magnetization recovery data of resolved peaks or were estimated from null points for incompletely resolved resonances of interest. Steady-state NOE measurements were

made using both a conventional (Donaire et al., 1994) and a super-WEFT pulse sequence. The selected resonance was irradiated for ~90% of the relaxation delay time. Data were acquired by interleaving a block of scans with saturation on-resonance with a block of equal scans with saturation off-resonance. The steady-state NOE (Neuhaus et al., 1989; La Mar & de Ropp, 1993) $\eta(j{\rightarrow}i)$, for an effectively relaxed proton *i* when proton *j* is saturated, is given by

$$\eta(j{\rightarrow}i) = \sigma_{ij}T_{1i} \qquad (1)$$

where T_{1i} is obtained from a nonselective inversion−recovery experiment, and σ_{ij} is the cross-relaxation rate given by

$$\sigma_{ij} = -0.1\gamma^4h^2r_{ij}^{-6}\tau_c \qquad (2)$$

with r_{ij} the interproton distance, and $\tau_c \sim 3$ ns can be assumed to be the rotational correlation time of the protein.

Phase-sensitive TOCSY (Bax & Davis, 1985) and NOESY (Jeener et al., 1979) spectra were recorded at 30 and 40 °C using mixing time of 15 and 60 ms for TOCSY and 50, 150, and 350 ms for NOESY over a 7017 Hz sweep width. The 60 ms TOCSY and 150 and 350 ms NOESY spectra consisted of 96 scans collected at a repetition rate of 0.5 s^{-1}, the 15 ms TOCSY consisted of 256 scans collected at a repetition rate of 1.3 s^{-1}, and the 50 ms NOESY consisted of 160 scans collected at a repetition rate of 0.7 s^{-1}; all with 2048 complex t_2 points over 512 t_1 blocks. The water signal was suppressed by low-power selective irradiation during the predelay period for all experiments, followed by a SCUBA sequence (Brown et al., 1988) to allow for magnetization recovery of resonances close to the water frequency.

NMR data were processed on either a Silicon Graphics Indigo workstation or a SUN Sparc station using the Biosym Felix 2.3 program. 30°-shifted sine-bell-squared functions were applied in both dimentsions for NOESY and TOCSY data. Data sets were zero-filled to 2048 × 2048 real data points prior to Fourier transformation.

RESULTS

pH and Temperature Effects on Ligated Cys. The complete 500 MHz ^1H NMR spectrum of *Pf* 3Fe Fd^{ox} in 90% ^1H_2O/10% ^2H_2O at 30 °C, pH 8.0, is shown in Figure 3. The previously investigated contact shifted and strongly relaxed Cys resonances are labeled $C_αH$, $C_βH$, and $C_{β'}H$, with $C_{β'}H$ defined as the more strongly relaxed, and hence the closer of the the two β-protons to the cluster iron. A combination of steady-state NOEs and relaxation measurements in ^2H_2O had led to the pairing of the resolved
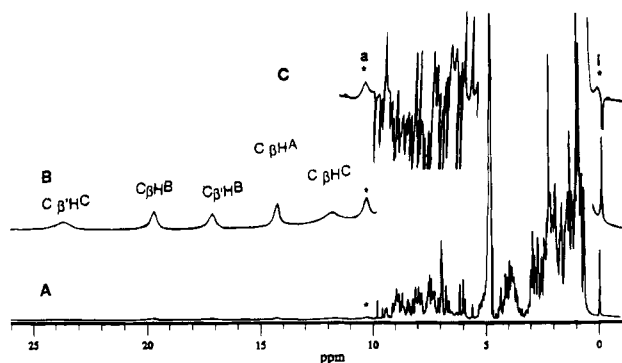
FIGURE 3: (A) 500-MHz 1H NMR spectra of *Pf* 3Fe Fd^{ox} in 90% 1H$_2$O/10% 2H$_2$O and 50 mM phosphate, pH 8.0, at 30 °C, collected under nonsaturating conditions (0.33 scans s^{-1}). (B) Vertically expanded section of the contact shifted and resolved signals for Cys A, B, and C are labeled C$_\beta$H, C$_\beta'$H, and C$_\alpha$H, where the closer to the cluster iron of β,β' is designated β' (Busse et al., 1992); the low-field peak labeled a arises from a relaxed labile proton. The upfield inset (C) of a partially relaxed spectrum (relaxation delay 10 ms) identifies a rapidly relaxed upfield labile proton peak i.
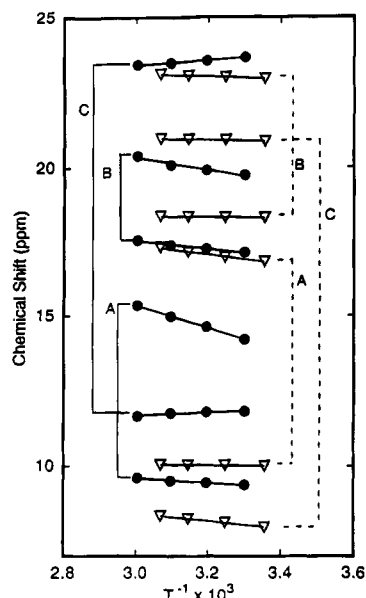

FIGURE 4: Plot of chemical shift, referenced to DSS, versus reciprocal absolute temperature (Curie plot) of the resolved C$_\beta$H, C$_\beta'$H, and C$_\alpha$H peaks for Cys A, B, and C (labeled in Figure 3) for *Pf* 3Fe Fd^{ox} at pH 8.0 (solid markers, solid lines) and at pH 3.4 (open markers, dashed lines) in 2H$_2$O at 30 °C. Note that while Cys A and B exhibit anti-Curie (negative slope) and Cys C display Curie-like (positive slope) behavior at pH 8.0, all three Cys exhibit anti-Curie behavior at low pH.

resonance to the three Cys labeled Cys A, Cys B, and Cys C; Cys A and B exhibit anti-Curie, and Cys C exhibited Curie-like, behavior in a plot of observed shift versus reciprocal temperature (solid lines in Figure 4) (Busse et al., 1992). The reversible pH behavior for these contact shifted Cys signals is displayed in Figure 5, with all peaks exhibiting an inflection consistent with the titration of a single proton with pK ∼5.2. The temperature dependence of the Cys resonances in the flat portion of the low pH region (pH 3.5) is included in Figure 4 (dashed lines), and it is observed that the peaks for all three Cys exhibit similarly weak anti-Curie behavior.

Cluster-Induced Relaxation. The 5.5−10.5 ppm window of the 500 MHz 1H NMR spectrum at 30 °C in 1H$_2$O, in which the labile protons are expected to resonate, is expanded
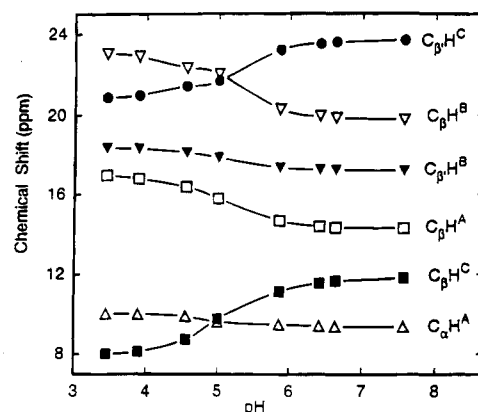

FIGURE 5: Plot of the chemical shift, referenced to DSS, for the resolved contact shifted C$_\beta$H, C$_\beta'$H, and C$_\alpha$H peaks for Cys A, B, and C (labeled in Figure 3), as a function of solution pH for *Pf* 3Fe Fd^{ox} in 2H$_2$O at 30 °C. The lines simply connect the points. The chemical shifts uncertainty is ±0.1 ppm and the pH uncertainty is 0.1 unit below pH 6. The obvious inflections observed for each line are consistent with the titration of a single proton with pK ∼5.2

in Figure 6A. The positions of the peptide NHs signals previously assigned in the conventional 2D spectra are labeled solely by residue number, amine side chain NH$_2$s are indicated by residue number with an asterisk, and the aromatic residue nonlabile side chains protons are labeled by residue number with dagger (Teng et al., 1994). The two relaxed C$_\alpha$H signals for Cys A and an unidentified C$_\alpha$H−C$_\beta$H−CH$_3$ fragment X are labeled C$_\alpha$H^A and C$_\alpha$H^X, respectively (Busse et al., 1992; Teng et al., 1994). Inspection of Figure 6A reveals several broad resolved or partially resolved labile protons labeled b, d, g, and h which were not previously detected in the conventional 2D NMR data (Teng et al., 1994). Two labile protons with short T_1s not shown in the expansion in Figure 6A are labeled a and i in Figure 3C. The nonselective spin−lattice relaxation times for both resolved or partially resolved labile and nonlabile protons obtained from the initial slope, or estimated from the null point, in an inversion−recovery experiment for detectable paramagnetically relaxed ($T_1 \leq 250$ ms) resonances, are listed in Table 1. A fast relaxing ($T_1 \sim 10$ ms) nonlabile proton peak r at 0.59 ppm with temperature independent shift (not shown; see Supplemental Material) is attributed to the methyl group near the cluster.

The WEFT NMR spectrum in this region, designed to suppress the intensity of all peaks with $T_1 \geq 400$ ms and to allow full relaxation of all protons with T_1s ≤ 40 ms, is shown in Figure 6B. The nonlabile protons C$_\alpha$H^A and C$_\alpha$H^X as well as the rapidly relaxed labile protons, b, d, g, h (Figure 6A), and a, i (not shown), appear with essentially full intensity in the WEFT trace. Also observed as fully relaxed (i.e., $T_1 \leq 50$ ms) are peaks previously assigned (Teng et al., 1994) to the NHs of Ile[61], Ala[18], and three unresolved protons not directly detected in Figure 6A and labeled c, e, and f in Figure 6B; each of the latter three signals is degenerate with one (or more) slowly relaxing NHs in Figure 6A, as evidenced by the signal intensities. Other NHs which exhibit significant residual intensity in the WEFT trace, and which likely exhibit $T_1 < 150$ ms, are Gln[34], Ser[19], and at least one of the ring protons of Phe[25] at 6.98 ppm (Busse et al., 1992). The positions of the rapidly relaxed protons, in particular peaks c and d, are better resolved in the partially relaxed NMR trace in Figure 6C.
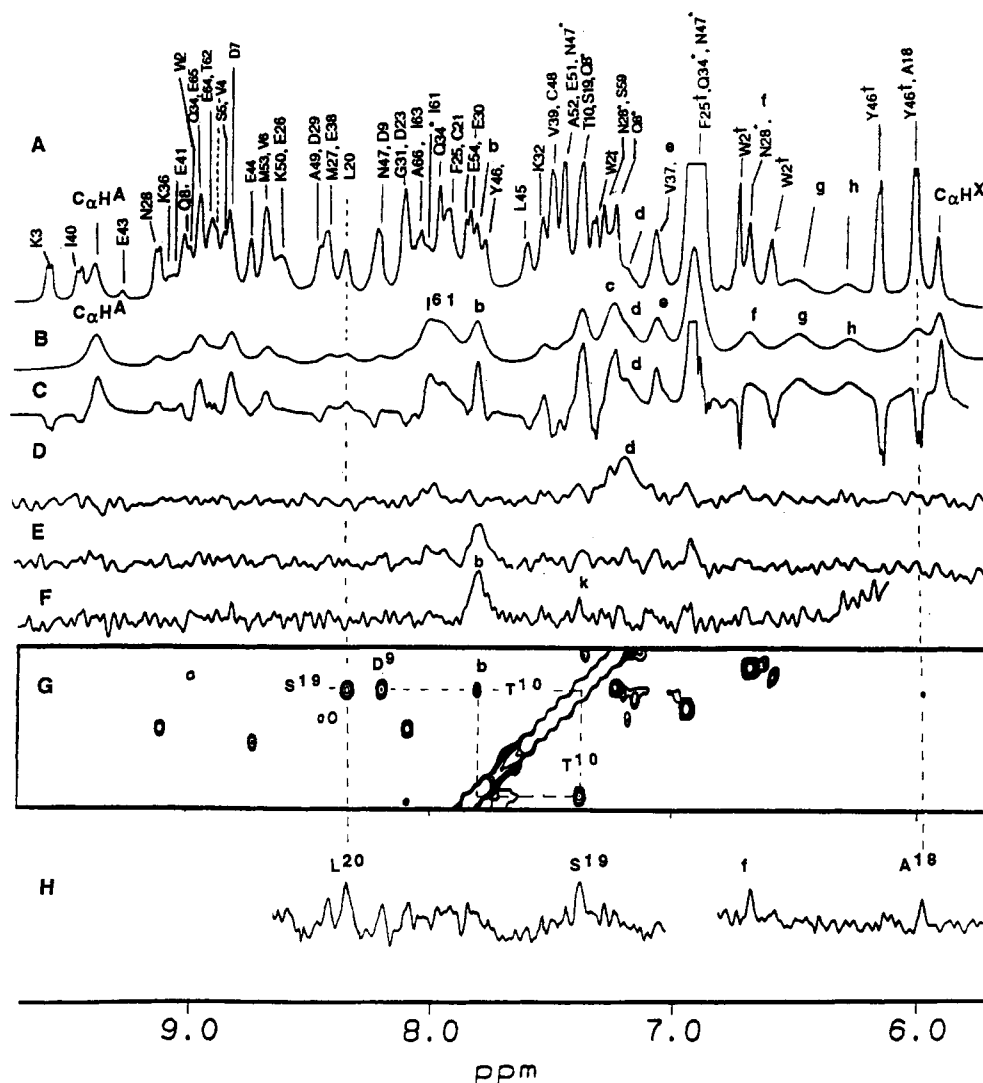
FIGURE 6: (A) Expanded portion of the 500-MHz ^{1}H NMR spectrum of *Pf* 3Fe Fd[ox] in 90% [1]H$_2$O/10% [2]H$_2$O at 30 °C, collected under nonsaturating conditions (0.33 scans s[−1]); previously assigned peptide NHs are labeled by one-letter amino acid and sequence number, amine groups are also marked by asterisks, and nonlabile aromatic ring protons by a dagger. The moderately relaxed nonlabile C$_\alpha$Hs of Cys A and an unidentified CH−CH−CH$_3$ fragment X are labeled C$_\alpha$H^A and C$_\alpha$H^X, respectively. Resolved or partially resolved labile proton peaks in the window not previously detected are labeled b, d, g, and h. (B) Super-WEFT trace in [1]H$_2$O (recycle time 333 ms, relaxation delay 67 ms) for the same spectral window that emphasizes fast relaxing protons, and completely suppresses slowly (T_1 > 400 ms) relaxing protons. Note the retention of essentially the complete intensity of C$_\alpha$H^A (T_1 ∼ 30 ms) and C$_\alpha$H^X (T_1 ∼ 35 ms) as well as for unidentified labile proton peaks b, c, d, e, f, g, h (also a and i, not shown), and the NHs of previously identified Ile[61] and Ala[18]. (C) Partially relaxed inversion-recovery spectrum in [1]H$_2$O (repetition rate 0.33 scans s[−1], relaxation delay of 175 ms) which establish the presence of fast relaxing, broad components under the narrow, slow relaxing peaks for peak f and Ala[18] NH. (D) Steady-state NOE in [1]H$_2$O to labile peak d (∼−2.5 ± 0.5%) upon ∼50% saturation of C$_\beta$H^B for 85 ms. Steady-state NOE upon saturating C$_\beta$'H^C (E) and C$_\beta$H^C (F) with each leading to a −2.5 ± 0.5% NOE to labile proton peak b. (G) Section of the NOESY spectrum in [1]H$_2$O with τ_m = 50 ms showing the cross peak between b and the NH of Thr[10] and/or Ser[19], which are degenerate at 30 °C. (H) Slice in the f_2 direction through the C$_\alpha$H^A diagonal in the τ_m = 50 ms [1]H$_2$O NOESY spectrum showing cross peaks to NHs of Ala[18], Ser[19], and Leu[20].

Steady-State NOEs to Labile Protons. Saturation of C$_\beta$'H^B in [1]H$_2$O leads to a −2.5 ± 0.5% NOE to labile proton peak d which is absent in a protein equilibrated in [2]H$_2$O (Figure 6D). A similar intensity NOE is detected when C$_\beta$H^B is saturated (not shown). The T_1 = 40 ± 10 ms of d translates to C$_\beta$H^B-d, C$_\beta$'H^B-d separations of 2.6 ± 0.2 Å using eqs 1 and 2. The line shape in Figure 6D reproducibly suggest two NOEs, with the low-field component much weaker (see below). Saturating the C$_\beta$H^C and C$_\beta$'H^C peaks (Figure 6F,E) similarly leads to a −2.5 ± 0.5% NOE to a labile proton peak b partially resolved in Figure 6A,B. The T_1(b) = 40 ± 10 ms translates to a similar internuclear separation of 2.6 ± 0.2 Å. A second, much weaker but reproducible NOE is detected in Figure 6F to peak k which aligns with the

previously assigned degenerate Thr[10] and Ser[19] NHs (Teng et al., 1994).

The labile proton peaks b and d are not resolved in the reference spectrum in [1]H$_2$O at 40 °C, but the resulting NOESY map is better resolved. Thus saturating C$_\beta$'H^C yields NOEs to both peak b and to peak k (Figure 7C). The patterns of steady-state NOEs to two labile protons, d and j, upon saturating C$_\beta$H^B (Figure 7E) and to only d upon saturation of C$_\beta$'H^B (Figure 7F) are also clearer at 40 °C. A moderately strong NOE is observed to a nonlabile proton peak p at 4.72 ppm upon irradiating C$_\beta$H^B (Figure 7E). Saturation of C$_\beta$H^A fails to exhibit NOEs to labile protons (not shown).

Steady-State NOEs to Nonlabile Protons. Steady-state NOEs from Cys C$_\beta$Hs and C$_\alpha$Hs to nonlabile protons are

Table 1: ¹H NMR Spectral Parameters for Active Site Residue Signals for Oxidized *Pf* 3Fe Fd

symbol	assignment	chemical shift (ppm)[a]	T_1 (ms)[b]
$C_\beta'H^C$	Cys¹¹ $C_\beta'H$	23.06	5
$C_\beta H^B$	Cys⁵⁶ $C_\beta H$	19.73	9
$C_\beta'H^B$	Cys⁵⁶ $C_\beta'H$	17.14	3
$C_\beta H^A$	Cys¹⁷ $C_\beta H$	14.27	9
$C_\beta H^C$	Cys¹¹ $C_\beta H$	11.82	11
a	NH^c	10.26	3
$C_\alpha H^A$	Cys¹⁷ $C_\alpha H$	9.37	30
	Gln³⁴ NH^d	8.91	<100
	Asp⁷ NH^d	8.80	
	Leu²⁰ NH^d	8.34	250
	Ile⁶¹ NH^d	7.98	30
b	Cys¹¹ NH	7.82	40
	Lys³² NH^d	7.52	200
k	Thr¹⁰ NH^d	7.37	
	Ser¹⁹ NH^d	7.37	<100
c	NH^c	7.24	
j	Ser⁵⁹ NH^e	7.28	<100
d	Cys⁵⁶ NH	7.19	40
e	NH^c	7.07	≤30
f	NH^c	6.69	≤30
g	NH^c	6.49	8
h	NH^c	6.27	3
	Ala¹⁸ NH^d	6.00	18
$C_\alpha H^X$	Val⁵⁸ $C_\alpha H$(?)	5.89	35
	Ala³³ $C_\alpha H^d$	5.58	45
$C_\beta'H^A$	Cys¹⁷ $C_\beta'H$	5.22	<10
	Thr¹⁰ $C_\alpha H^d$	4.13	
p	Ser⁵⁹ $C_\alpha H^d$	4.72	
	Thr¹⁰ $C_\beta H^d$	3.86	
t	Gln⁸ $C_\alpha H$(?)	3.80	
v	Met⁵³ $C_\alpha H$(?)	3.80	
m	Ile¹⁶ $C_\beta H$(?)	3.78	
	Lys³² $C_\varepsilon H^d$	2.99	
	Phe²⁵ $C_\beta H^d$	2.78	
	Phe²⁵ $C_\beta'H^d$	2.30	~50^f
	Lys³² $C_\beta H^d$	1.72	
	Leu²⁰ $C_{\beta 2}H^d$	1.72	
	Leu²⁰ $C_{\beta 1}H^d$	1.62	
n	Ile¹⁶ $C_\gamma H_3$ (?)	1.13	
	Ala⁵² $C_\beta H_3^d$	1.26	
s	Ile¹² CH₃ (?)	1.10	
	Leu²⁰ $C_\delta H_3^d$	0.79	
r	Ile⁶¹ $C_\delta H_3$(?)	0.59	15
i	NH^c	0.16	<3

[a] Chemical shifts in ppm from DSS, in ¹H₂O at 30°C, pH 8. [b] For resolved and partially resolved resonances, uncertainty ±20%. [c] Not assigned, but established to be labile protons. [d] Shift data taken from Teng et al. (1994). [e] Chemical shift reported incorrectly in Teng et al. (1994). [f] The T_1 is dictated by the fact that the $C_\beta H–C_\alpha H$ NOESY cross peaks intensity is maximum near $\tau_m = 50$ ms, and $C_\beta H'$ is closer to the cluster in *Dg* Fd.

better defined in ²H₂O solution, as shown in Figure 8. Saturating $C_\alpha H^A$ (which cannot be saturated in ¹H₂O; see Figure 6A), exhibits moderate intensity NOEs to Leu²⁰ $C_{\beta 1}H$, $C_{\beta 2}H$, and $C_{\delta 1}H_3$, weak NOEs to Ala⁵² $C_\beta H_3$ and the Phe²⁵ ring, and strong NOEs to two protons not previously identified in the 2D maps (labeled m and n in Figure 8A). Saturation of $C_\beta H^A$, in addition to the previously reported NOEs to $C_\alpha H^A$ and the Phe²⁵ ring (Busse et al. 1992), yields moderate intensity NOEs to the $C_\beta Hs$ of Phe²⁵ and a weak and strong NOE to the m and n protons, respectively (Figure 8B). Saturation of $C_\beta'H^C$ (Figure 8C) and $C_\beta H^C$ (Figure 8D) in ²H₂O more clearly exhibits the intense NOE to a peak t at the frequency of both the Gln⁸ and Met⁵³ $C_\alpha H$, weak NOEs to moderately relaxed peaks previously identified as $C_\varepsilon H$ and $C_\beta H$ of Lys³², and a peak s at 1.1 ppm not previously detected in 2D maps (Teng et al., 1994). Irradiation of $C_\beta'H^B$ (Figure 8E) and $C_\beta H^B$ (Figure 8F) yields moderate NOEs to peak v at a chemical shift of the degenerate $C_\alpha Hs$ of Gln⁸ and Met⁵³

as well as a weak NOE to the broad and relaxed apparent methyl peak r at 0.59 ppm.

2D Spectra in ¹H₂O. The majority of the relaxed labile protons detected in the spectra in Figure 6A,B do not contribute cross peaks to NOESY or TOCSY spectra collected at long mixing times needed to optimally characterize the major portion of the protons away from the cluster ($\tau_m \geq 60$ ms for TOCSY and $\tau_m \geq 150$ ms for NOESY). Notable exceptions are the weak TOCSY connectivities that identified the relaxed Ile⁶¹ and Ala¹⁸ NHs (Teng et al., 1994). However, when NOESY spectra are collected with $\tau_m = 50$ ms with an increase in the number of scans, weak but crucial cross peaks are detected to several of the relaxed labile protons. The section of the 50 ms NOESY map at 30 °C in Figure 6G reveals a cross peak between peak b and peak k, the NH of either Thr¹⁰ or Ser¹⁹. Peak b is not resolved in the reference trace at 40 °C, but the degeneracy between Thr¹⁰ and Ser¹⁹ is lifted, clearly identifying[2] the cross peak as between Cys^C NH (b) and Thr¹⁰ NH (k) (Figure 7B). The previously unidentified proton signal s (Figure 7C) at 1.1 ppm exhibits a single weak NOESY cross peak at $\tau_m = 50$ ms, but not at 150 ms, that also exhibits a cross peak to Thr¹⁰ $C_\alpha H$ (Figure 7A″). The portion of the $\tau_m = 60$ ms TOCSY map (Figure 7D) locates the NH, $C_\alpha H$, and $C_\beta Hs$ of the weakly relaxed residue Ser⁵⁹ identified previously (Teng et al., 1994). The alignment with the steady-state NOEs to j and p from $C_\beta H^B$ at 40 °C (Figure 7E) shows they arise from the NH and $C_\alpha H$, respectively, of Ser⁵⁹.

Lastly, the resolved $C_\alpha H^A$ peak is too close to labile protons to saturate in ¹H₂O (Figure 6A). However, the 30 °C NOESY map in ¹H₂O with $\tau_m = 50$ ms exhibits a number of weak cross peaks to labile protons in a slice through $C_\alpha H^A$ which are not present for $\tau_m = 150$ ms (not shown), as illustrated in Figure 6H. These weak cross peaks are identified as the strongly relaxed NH of Ala¹⁸ and the weakly relaxed NHs of Ser¹⁹ and Leu²⁰, as well as to the unidentified strongly relaxed NH signal f.

TOCSY and NOESY spectra at both short and long mixing times reveal cross peaks between the signal m and n that exhibit strong NOEs to $C_\beta H^A$ and $C_\alpha H^A$; however, no additional TOCSY cross peaks are observed to m and n down to $\tau_m = 15$ ms, and the only additional NOESY cross peak at $\tau_m = 50$ ms is detected between m and the peptide NH of Met⁵³ (not shown; see Supplementary Material). The resolved and moderately relaxed ($T_1 \sim 35$ ms) peak $C_\alpha H^X$ in Figure 6A has been shown to exhibit scalar cross peaks to 2.62 and 1.38 ppm indicative of a $C_\alpha H–C_\beta H–C_\gamma H_3$ fragment (residue X) from a Val or an Ile (Teng et al., 1994). This $C_\alpha H^X$, however, fails to exhibit any detectable additional NOESY cross peaks to aid in its identification. Other isolated cross peaks are observed in the 15 ms TOCSY and 50 ms NOESY maps at 30 and 40 °C (not shown), which corresponded to proton frequencies not identified in the long mixing time maps,[3] but none of these protons could be

---

[2] A NOESY cross peak between Cys¹¹ NH and Thr¹⁰ $C_\beta H$ is also observed in Figure 7A. This $\beta_i–N_{i+1}$ dipolar connectivity is unusual, but appears real, and it is also observed in the related *Thermococcus literalis* 4Fe Fd (A. Donaire, unpublished data). Hence, this dipolar connection may reflect the nature of the turn that terminates with the first ligating Cys in these related Fd.

[3] Several spin systems detected by weak TOCSY peaks but which could not be assigned previously were found to result from minor products due to oxidation damage to the protein.
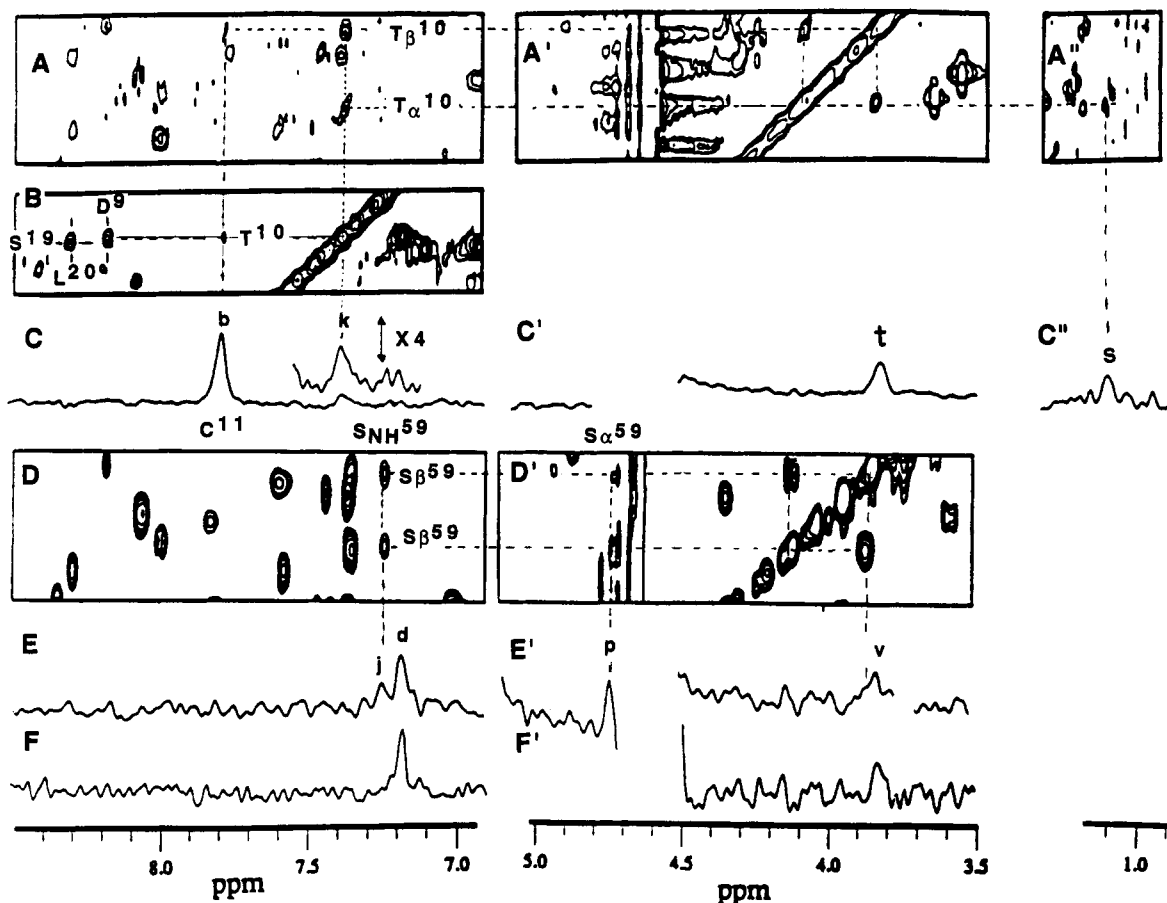
FIGURE 7: (A, A', A'', B) Portions of the NOESY spectrum with $\tau_m = 50$ ms for *Pf* 3Fe Fd^{ox} in ^1H_2O at 40 °C illustrating cross peaks from Cys^{11} NH (peak b) to Thr^{10} NH (k) and C$_\beta$H. (C, C') Steady-state NOE in ^1H_2O at 40 °C upon saturating C$_\beta'$H^C for 85 ms to both peak b and Thr^{10} NH (k) which is now resolved from Ser^{19} NH. The NOEs to t correspond to C$_\alpha$H of Glu^8 or Met^{53}, and peak s to a methyl of an Ile on the loop between Cys I and Cys III. (D, D') Sections of the TOCSY spectrum with $\tau_m = 60$ ms showing the scalar connectivity for the weakly relaxed Ser^{59}. (E, E') Steady-state NOE at 40 °C upon saturating C$_\beta$H^B to labile peak d, as well as to both the NH (j) and C$_\alpha$H (p) of Ser^{59}; the NOE to v is to C$_\alpha$H of either Glu^8 or Met^{53}. (F, F') Saturation of C$_\beta'$H^B fails to exhibit NOEs to either NH or C$_\alpha$H of Ser^{59}.

uniquely correlated to an assigned proton with the available data.

DISCUSSION

Sequence-Specific Assignment of Cys. The available steady-state NOEs from the Cys C$_\beta$Hs, together with the short mixing time NOESY data, allow not only the unambiguous sequence-specific assignments of the ligated Cys in the same fashion as pursued for a diamagnetic protein [i.e., via backbone connectivities (Wüthrich, 1986)] but provide important information on qualitatively conserved aspects of the cluster ligating geometry. This approach, moreover, is suggested to have broad applicability for the cubane cluster Fd. Thus inspection of the crystal structures of the available bacterial-type Fd, i.e., 3Fe *Dg* Fd, 2 × 4Fe *Peptococcus aerogenes (Pa)* Fd, 4Fe *Bacillus thermoproteolyticus (Bt)* Fd, and 3Fe/4Fe *Azotobacter vinlandii (Av)* Fd (Kissinger et al., 1991; Adman et al., 1976; Fukayama et al., 1988; Stout, 1989; Backes et al., 1991), reveals a largely conserved pseudosymmetry among the four cluster ligands of a given cluster,[4] labeled Cys I−IV, where Cys I and Cys IV invariably have their C$_\alpha$Hs oriented toward the ligating iron ($R_{Fe} \sim 3.3 \pm 0.3$ Å), but with their peptide NHs oriented away from the cluster ($R_{Fe} \sim 5.5 \pm 0.3$ Å). Conversely, Cys II (except in *Dg* 3Fe Fd and cluster no. 2 in *Av* FD, where Cys II is not ligated) and Cys III have their C$_\alpha$Hs

pointed away from the cluster ($R_{Fe} \sim 5.3 \pm 0.3$ Å), while the peptide NH point toward the cluster ($R_{Fe} \sim 3.2 \pm 0.3$ Å), as shown qualitatively in Figure 1.

On the basis of the relaxation properties of the two C$_\beta$Hs ($T_1 \sim 2-10$ ms), which are ~ 3.3 to ~ 4.2 Å from the iron (Busse et al., 1992), it would be expected that NHs from Cys I and IV should have T_1s = $30-60$ ms and would exhibit NOESY cross peaks at $\tau_m \sim 50$ ms, while the NHs of Cys II and III would be too severely relaxed ($T_1 \leq 3$ ms) to exhibit such NOESY cross peaks. Similarly, the C$_\alpha$H orientations predict only moderately relaxed ($T_1 = 30-40$ ms) signals capable of exhibiting detectable NOESY cross peaks for Cys II and III, but too strongly relaxed ($T_1 < 5$ ms) NH peaks for Cys I and IV. The expected detectable peptide NHs of Cys I and IV are found similarly close ($2.6-3.0$ Å) to each of the C$_\beta$Hs of the same Cys in each of these crystal structures, thereby providing a route to identifying the NHs. Therefore, if the cluster architecture is approximately conserved, the NHs of Cys I and IV and the C$_\alpha$Hs of Cys II and III should be only moderately relaxed

---

[4] In the 2 × 4Fe *Pa* Fd (Adman et al., 1976) and 4Fe:3Fe *Av* Fd (Stout, 1988), Cys I−IV are defined the same as for *Dg* and *Pf* Fd in Figure 2. Cys I−IV for the second clusters are those reflected by the pseudo-2-fold symmetry of the *Pa* Fd, i.e., Cys 8, 11, 14, and 46 for the cluster homologous to *Dg* and *Tl* Fd, and Cys 36, 39, 42, and 18, respectively, for the second cluster.
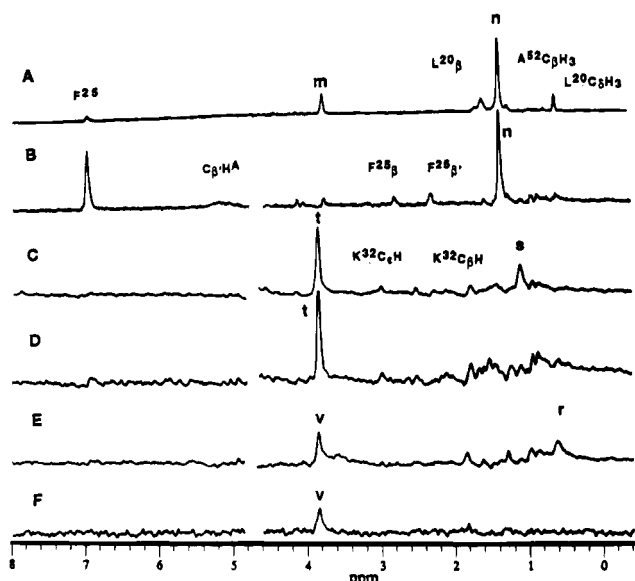
FIGURE 8: Steady-state NOEs for the resolved Cys resonance of *Pf* 3Fe Fd^{ox} in ^2H_2O at 30 °C, pH 8.0. (A) Saturate C$_\alpha$H^A; note NOEs to previously identified Phe^{25} ring, Leu^{20} C$_\beta$H, C$_\beta$'H, C$_\delta$H$_3$, Ala^{52} C$_\beta$H$_3$, and unidentified peaks m and n (which exhibit a TOCSY cross peak between them). (B) Saturate Cys C$_\beta$H^A; note NOEs to Phe^{25} ring, C$_\beta$'H^A, Phe^{25} C$_\beta$H, and C$_\beta$'H as well as to m and as n seen for C$_\alpha$H^A above. Saturate C$_\beta$'H^C (C) and C$_\beta$H^C (D); note common NOEs to Lys^{32} C$_\epsilon$H, C$_\beta$H, and peak t (C$_\alpha$H of either Glu^8 or Met^{53}). Saturate C$_\beta$'H^B (E) and C$_\beta$H^B (F); note NOEs to peak v (C$_\alpha$H of either Met^{53} or Glu^8) as well as NOE for C$_\beta$'H^B to r.

and can be expected to contribute to appropriately tailored 1D and 2D spectra.

The steady-state NOEs from both of the C$_\beta$Hs for each of Cys C and B to the labile proton peaks b and d, respectively, indicate a separation of ~2.6 Å between the NH and the two C$_\beta$Hs for each Cys, and hence identify the peptide NHs from Cys C and Cys B, respectively. The expectation of conserved cluster architecture, (as depicted in Figure 1) alone demands that the pair Cys B, C arise from the pair Cys I, IV (which are Cys^{11}, Cys^{56} in *Pf* Fd). The diagnostic backbone NOESY cross peak between peak b and the peptide NH of Thr^{10} uniquely establishes the origin of Cys C as Cys^{11}(I). This is further confirmed[2] by the weak direct NOE from the Cys^{11}(I) C$_\beta$H to Thr^{10} NH (k) (Figure 7C). The Cys B peptide NH (peak d) fails to exhibit a NOESY cross peak to another labile proton. However, it is adjacent to the severely relaxed Pro^{57}, and neither Val^{58} nor Ala^{55} NHs have been detected (Teng et al., 1994). The steady-state NOEs from C$_\beta$H^B to both the NH (j) and C$_\alpha$H (p) of Ser^{59} (Figure 7E) however, establish unequivocally that the Cys B arises from Cys^{56}(IV). The C$_\alpha$Hs from neither Cys^{11}(I) nor Cys^{56}(IV) could be detected, consistent with the expected extreme relaxation properties.

Lastly, the C$_\alpha$H, but not the NH, of the remaining Cys A is detected with relaxation properties consistent with the expectation for Cys II or III in the structure in Figure 1. The assignment of Cys A to the remaining Cys^{17} is independently confirmed by the backbone NOESY cross peak for C$_\alpha$H^A to the peptide NHs of Ala^{18}, among others (see below), as shown in Figure 6H.

Previous assignments of the ligated Cys resonances in *Thermococcus litoralis* (*Tl*) 4Fe Fd based on an assumed conserved tertiary structure relative to *Dg* Fd had shown that

Cys II and III indeed exhibit the expected (T_1 ~ 30 ms) relaxation properties for C$_\alpha$Hs (Donaire et al., 1994). Preliminary studies[5] on the 4Fe form of both *Pf* and *Tl* Fd indicate that this strategy for sequence-specific assignments of contact shifted Cys resonances using the readily detectable NHs of Cys I and IV and C$_\alpha$Hs of Cys II and III has very general applicability in cubane cluster Fds.

Magnetic Asymmetry. The assignments above identify Cys C = Cys^{11}(I) as uniquely exhibiting Curie-like temperature dependence, and pairs Cys A = Cys^{17}(III) and Cys B = Cys^{56}(IV), both of which display anti-Curie behavior at alkaline pH, as shown in Figure 4 (Busse et al., 1992). The structural basis for an apparent stronger spin coupling between Cys^{11}(I) and Cys^{17}(III) than between Cys^{56}(IV) and either Cys^{11}(I) and Cys^{17}(III) (Macedo et al., 1993a) is not known at this time but may become apparent when a more complete structure for this protein becomes available. However, it is noted that the magnetic pairing in 3Fe *Pf* Fd is not the same as that reported for the oxidized 3Fe Fd for *Dg* and *Tl* Fd (Macedo et al., 1993b; Donaire et al., 1994), both of which identified the magnetically unique iron as ligated to Cys IV.

It is noted, moreover, that the ligated Cys contact shifts in *Pf* 3Fe Fd^{ox} reflect the titration of a residue with pK ~5.2, as shown in Figure 5. The origin of the titrating residue is tentatively proposed to be the nonligated Asp^{14} homologous to Cys II in the cluster binding consensus sequence, based on the absence of the pH influence on the ¹H NMR spectra of the 4Fe *Pf* Fd^{ox} where Asp^{14} is ligated to the cluster.[6] Perhaps more interestingly, the protonation has the effect of abolishing the magnetic 2:1 asymmetry of the cluster. At low pH, the contact shift for all three Cys exhibit very similar weak anti-Curie temperature dependence (Figure 4) indicating that all magnetic couplings are essentially the same. The suppression of the magnetic asymmetry at low pH is also reflected in the changes in the magnitude of the spin magnetizations on the individual iron atoms, with those exhibiting anti-Curie behavior [Cys A,B or Cys^{17}(III), Cys^{56}-(IV)] experiencing increases, while that displaying Curie-like behavior [Cys^{11}(I)] experiences a decrease in contact shift at low relative to high pH.

Secondary Structure Near the Cluster. Crystallographically characterized *Dg* 3Fe Fd exhibits a short α-helix which includes the ligating Cys III and terminates in β-turn C, as well as β-turn E which is initiated by the ligating Cys IV, as reproduced schematically in Figure 2A (Kissinger et al., 1991). Previous 2D NMR experiments designed to optimally provide information on the overall folding topology failed to provide direct information on either of these secondary structural elements because of adverse cluster relaxation influences (Teng et al., 1994).

The NMR experiments designed for detecting rapidly relaxed proton signals strongly support the conservation of α-helix A. Thus, the slice for Cys^{17}(III) C$_\alpha$H^A in the 50 ms NOESY map (Figure 6H) not only exhibits the backbone cross peak to the NH of Ala^{18} that assign the residue but also yields detectable cross peaks to the peptide NHs of Ser^{19} and Leu^{20}, which are characteristic of the α$_i$–N$_{i+1}$, α$_i$–N$_{i+2}$,

[5] A. Donaire, G. N. La Mar, Q. Teng, Z. H. Zhou, and M. W. W. Adams, unpublished data.

[6] C. M. Gorst, G. N. La Mar, and M. W. W. Adams, unpublished observations.

and $\alpha_i - N_{i+3}$ connections on a helix (Wüthrich, 1986). The reduced intensity of the cross peaks, particularly from Cys[17] $C_\alpha H^A$ to NH of Ala[18], is due to the severe relaxation for both protons (Table 1). The origin of the weak NOE to the strongly relaxed labile proton peaks f cannot be determined at this time. The helical motif is further supported by the diagnostic $\alpha_i - \beta_{i+3}$ NOEs observed in ^2H_2O between Cys[17] and Leu[20] (Figure 8A). The conserved orientation of the helix A with respect to the previously described β-turn B (Figure 2), as found in *Dg* Fd, is confirmed by the characteristic NOESY cross peak between Ala[18] $C_\beta H_3$ to Cys[21] C_βHs observed previously (Teng et al., 1994).

β-Turn E near the carboxy terminus in *Dg* Fd is initiated at the ligating Cys[50](IV) and involves the residues through Glu[53] (Figure 2A,B). This portion of the sequence in *Pf* Fd consists of Cys[56](IV) through Ser[59] and reflects conservative substitution (Figure 2C). Previously, only the signals of Ser[59] had been assigned in this segment, with the remainder of the adjacent residues severely relaxed by the cluster (Teng et al., 1994). The present assignment of Cys[56](IV), however, provides some direct support for the presence of β-turn E. Thus the *Dg* Fd structure predicts that the $C_\beta H$ (further from the iron) for Cys IV (but not the $C_\beta'H$ closer to the iron) is close to both the NH (3.2 Å) and $C_\alpha H$ (3.0 Å) of the fourth residues toward the carboxy terminus (Glu[53] in *Dg* Fd, Ser[59] in *Pf* Fd). These are precisely the dipolar contacts detected in the steady-state NOEs between Cys[56] $C_\beta H$ and the Ser[59] NH−$C_\alpha H$ fragment, as shown in Figures 7E. Thus β-turn E for Cys[56](IV) through Ser[59] appears to be conserved. However, the orientation of β-turn E relative to the remainder of the cluster may be different than in *Dg* Fd, since the long helix B in *Pf* Fd terminates before Cys IV (Figure 2D), while in *Dg* Fd, Cys[50](IV) is at the end of the helix B (Figure 2A).

Cluster Tertiary Contacts. The steady-state NOEs from Cys[17](III) $C_\beta H$ (Figure 8B) but not $C_\alpha H$ (Figure 8A) to Phe[25] C_βHs (2.8 and 2.0 Å) are those expected on the basis of *Dg* Fd crystal structure, confirming a conserved relationship between the cluster and the hydrophobic core (Kissinger et al., 1991). A moderate intensity NOE is expected from Cys 17(III) $C_\beta H$ to $C_\beta H_3$ of Ala[52] on the basis of the close proximity (3.0 Å) between the homologous Cys[14](III) and Ala[46] in *Dg* Fd (see Figure 2). However, only a very weak NOE observed in Figure 8A. Since the Ala[52] $C_\alpha H - C_\beta H_3$ TOCSY and NOESY cross peaks are strong at long mixing times, Ala[52] $C_\beta H_3$ is not being relaxed effectively by the cluster. Instead, it appears that Ala[52], near the C-terminus portion of α-helix B (Figure 2D), is farther from the cluster in *Pf* than *Dg* Fd.

The strong NOEs for Cys[17](III) $C_\beta H$ and $C_\alpha H$ to an apparent CH−CH$_3$ fragment of an Val or Ile (consisting of signals m and n) do not arise from any of the previously characterized residues (Teng et al., 1994). In fact, the failure to detect further TOCSY cross peaks to this fragment indicate that m and n arise from a relaxed residue near the cluster. Since NOEs are not observed to either Ser[59] nor Cys[56], the fragment is unlikely to arise from the only unidentified Val[58] but could arise from $C_\beta HC_\gamma H_3$ of unassigned Ile[12] or Ile[16] (Teng et al., 1994). The only other contact observed for this fragment is a weak NOESY peak at $\tau_m = 50$ ms from m to Met[53] NH (not shown; see Supplementary Material). This contact favors the assignment of m and n to $C_\beta H \, C_\gamma H_3$ of Ile[16] rather than Ile[12].

Cys[8](I) in *Dg* 3Fe Fd is predicted to be close to the side chain Lys[30] on the inner β-sheet B, with the Cys[8](I) $C_\beta'H$ but not $C_\beta H$, close to the Lys[30] $C_\epsilon H$, $C_\beta H$ (Kissinger et al., 1991). The weak NOEs from Cys[11](I) C_βHs to the Lys[32] $C_\epsilon H$ and $C_\beta H$ confirm the proximity of the β-sheet B to the cluster, but the observation of similar NOEs from both Cys[11]-(I) $C_\beta H$, $C_\beta'H$ suggests a slight rotation of the ligating Cys. This minor change may reflect the presence of an insertion just before Cys I in *Pf* Fd relative to *Dg* Fd (Figure 2). The NOE to peak s likely reflects a methyl on the adjacent Ile[12] based on its NOESY cross peak to Thr[10] $C_\alpha H$ (Figure 7A″). The NOE for Cys[56] (IV) $C_\beta'H$ to the frequency of peak r ($T_1 \sim 10$ ms) is that expected for Ile[61] $C_\delta H_3$, which is close to the cluster iron in the homologous Ile[56] in *Dg* Fd. Tentative identification of portions of Ile[12] and Ile[16] dictates that the $C_\alpha H - C_\beta H - CH_3$ fragment X more likely arises from Val[58] (see below). The remaining tertiary dipolar contacts for Cys[11](I), as well as those for Cys[56](IV), are more difficult to assign definitively. Both Cys exhibit strong to moderate interactions to the same frequency (peaks t and v) at which both Gln[8] and Met[53] $C_\alpha H$ are degenerate over the temperature range 10−55 °C (Teng et al., 1994). The folding topology of *Dg* Fd, together with the demonstrated structural homology for major portions of *Pf* Fd, indicate that the NOE for Cys[11]-(I) should be to Gln[8] $C_\alpha H$ (peak t), while that from Cys[56]-(IV) is to Met[53] (peak v). The latter contact is consistent with distances (3.2 Å) to the homologous residue[7] in *Dg* Fd (Ile[47]). It is clear, however, that more extensive 2D NMR data over a wider temperature range, and/or ^{15}N labeling, are necessary to unambiguously assign the remainder of the resonances.

Cluster Relaxation Influences. The strong discrimination in relaxation properties among the protons illustrated in the comparison of Figure 6 panels A and B, for which estimates of T_1 could be determined from the selected resolved resonances, provides independent qualitative information on the tertiary structure near the cluster. Under ideal conditions, the relaxation rates could be quantitatively analyzed to provide strong constraints for building a computer model for the Fd structure. However, a quantitative model for interpretation of dipolar relaxation induced by a spin-coupled chromophore in terms of distances to the metal centers (Banci et al., 1991) has not been tested. Our qualitative model is based on the assumption of a single electron spin relaxation time and approximately equal spin magnetization of each of the three irons, as reflected in their similar contact shifts (Busse et al., 1992; Macedo et al., 1993a). Since many protons are close to more than one iron in the center, the relaxation contributions over the three iron atoms are additive for each proton. These effects can be approximated by the relaxation

$$T_1^{-1} = D_q \Sigma R_q^{-6} \qquad (3)$$

where D is a constant because of a single T_{1e} and assumed equal distribution of spin magnetization, and R_q is the distance to each of the three iron atoms, $q = I$, III, and IV in Figure 1 (ligated to Cys I, Cys III, and Cys IV, respectively). A plot of the T_1^{-1} for predominantly paramagnetically relaxed protons ($T_1 \leq 250$ ms) in *Pf* 3Fe Fd^{ox}

---

[7] The likely efficient relaxation of peaks v and t is reflected in the significant intensity of this portion of the WEFT trace (not shown).
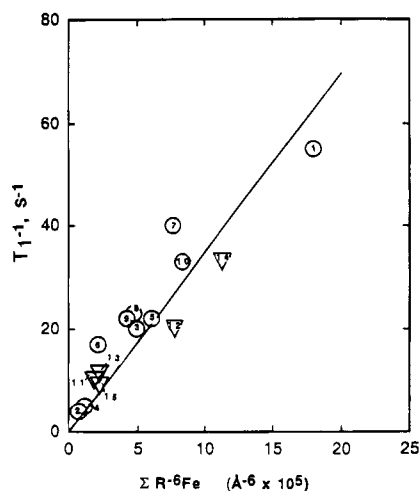
FIGURE 9: Plot of the estimated relaxation rate (T_1^{-1}) for resolved/ partially resolved and paramagnetically relaxed protons of *Pf* 3Fe Fd in ^1H_2O as a function of the sum of the inverse sixth power of the distance to each of the three iron (ΣR_i^{-6}) for the homologous protons in the crystal structure of *Dg* 3Fe Fd[ox]. The numbered points are as follows: 1, Ala[18] NH; 2, Leu[20] NH; 3, Phe[25] $C_{\beta}2H$; 4, Leu[32] NH; 5, Ala[33] $C_\alpha H$; 6, Val[58] $C_\alpha H$; 7, Ile[61] NH; 8, Cys[11] NH; 9, Cys[56] NH; 10, Cys[17] $C_\alpha H$; 11, Cys[11] $C_\beta H$; 12, Cys[11] $C_\beta'H$; 13, Cys[56] $C_\beta H$; 14, Cys[56] $C_\beta'H$; 15, Cys[17] $C_\beta H$. The horizontal scale for peaks 1−10 is that shown; both scales for peaks 11−15 (the hyperfine shifted peaks) are reduced by ×10 compared to those for peaks 1−10.

against the ΣR^{-6} calculated for the coordinates for homologous protons in *Dg* 3Fe Fd is shown in Figure 9.

The qualitative correlation between relaxation rates and proximity to the cluster, as represented in eq 3, can be taken as further support for conserved aspects of the tertiary structure relative to *Dg* Fd. Thus the Ala[33] $C_\alpha H$ on β-sheet B is well predicted, and the proximity to the cluster of the unresolved Glu[34] NH accounts for its intensity of the WEFT-trace in Figure 6B. The proximity to the iron of the Ile[61] NH (Ile[56] in *Dg*), as well as the tentataively assigned Val[58] $C_\alpha H$ ($C_\alpha H^X$ in Figure 6A, 6B), are also reasonably predicted. The analysis of the relaxation data as a structural constraint in building a molecular model appears promising, but further work to refine the model (i.e., asymmetric distribution of spin density that accounts for magnetic asymmetry in Figure 4) is required to test the validity of the approach on Fds for which the crystal coordinates are available. The analysis of the peptide NHs appears particularly promising because of the improved prospects for resolution of numerous assignable signals over a range of temperatures.

CONCLUSIONS

Spectral editing based on the differential relaxation of protons near the cluster allow the detection of the majority of the peptide NHs, and multipulse 1D and 2D experiments appropriately tailored to specific relaxation times should be capable of producing the correlation to weakly relaxed and assigned protons necessary to make assignments and deduce structure. The apparent conserved cluster ligation geometry allows a rational approach to the unique sequence-specific assignment of ligated residues in cubane cluster Fds which are independent of any assumptions of tertiary structure. In fact, the success of the present assignment strategy provides important verification for the approximate conservation of the ligating geometry in *Pf* Fd. The presently described approach to Cys assignments has general application to all

cubane Fds and may have use in directly assigning the sequence origin of the ligated Cys for the ferrous ion in 2Fe reduced Fd (Dugad et al., 1990; Skjeldal et al., 1991). Although more extensive 2D experiments over a wide range of conditions will be needed to assign the remainder of the cluster environment, the prospects for attaining the assignments and the spatial constraints through either $^1H-{}^1H$ dipolar correlation or paramagnetic relaxation needed to generate a robust molecular model by distance geometry and molecular dynamics, appear promising. Studies to extend such assignments, including ^{15}N labeling as well as development of a molecular model, are in progress.

SUPPLEMENTARY MATERIAL AVAILABLE

Two figures showing a portion of a 500-MHz NOESY spectrum of *Pf* 3Fe Fd[ox] and portions of an inversion−recovery experiment for *Pf* 3Fe Fd[ox] (2 pages). Ordering information is given on any current masthead page.

REFERENCES

Adman, E. T., Sieker, L. C., & Jensen, L. H. (1976) *J. Biol. Chem. 251*, 3801−3806.

Aono, S., Bryant, F. O., & Adams, M. W. W. (1989) *J. Bacteriol. 171*, 3433−3439.

Backes, G., Mino, Y., Loehr, T. M., Meyer, T. E., Cusanovich, M. A., Sweeney, W. V., Adman, E. T., & Sanders-Loehr, J. (1991) *J. Am. Chem. Soc. 113*, 2055−2064.

Banci, L., Bertini, I., & Luchinat, C. (1990) *Struct. Bonding 72*, 113−135.

Banci, L., Bertini, I., & Luchinat, C. (1991) in *Nuclear and Electron Relaxation*, pp 143−162, VCH, Weinheim, Germany.

Banci, L., Bertini, I., Capozzi, F., Carloni, P., Ciurli, S., Luchinat, C., & Piccioli, M. (1993) *J. Am. Chem. Soc. 115*, 3431−3440.

Bax, A., & Davis, D. G. (1985) *J. Magn. Reson. 65*, 355−360.

Beinert, H. (1990) *FASEB J. 4*, 2483−2494.

Bertini, I., Lanini, G., & Luchinat, C. (1984) *Inorg. Chem. 23*, 2729−2730.

Bertini, I., Briganti, F., Luchinat, C., Scozzafava A., & Sola, M. (1991) *J. Am. Chem. Soc. 113*, 1237−1245.

Bertini, I., Briganti, F., Luchinat, C., Messori, L., Monnanni, R., Scozzafava, A., & Vallini, G. (1992a) *Eur. J. Biochem. 204*, 831−835.

Bertini, I., Capozzi, F., Ciurli, S., Luchinat, C., Messori, L., & Piccioli, M. (1992b) *J. Am. Chem. Soc. 114*, 3332−3340.

Bertini, I., Capozzi, F., Luchinat, C., & Piccioli, M. (1993) *Eur. J. Biochem. 212*, 69−78.

Bertini, I., Capozzi, F., Luchinat, C., Piccioli, M., & Vila, A. J. (1994) *J. Am. Chem. Soc. 116*, 651−660.

Bominaar, E. L., Borshch, S. A., & Girerd, J. (1994) *J. Am. Chem. Soc. 116*, 5362−5372.

Brown, S. C., Weber, P. L., & Müller, L. (1988) *J. Magn. Reson. 77*, 166−169.

Busse, S. C., La Mar, G. N., & Howard, J. B. (1991) *J. Biol. Chem. 226*, 23714−23723.

Busse, S. C., La Mar, G. N., Yu, L. P., Howard, J. B., Smith, E. T., Zhou, Z. H., & Adams, M. W. W. (1992) *Biochemistry 31*, 11952−11962.

Cammack, R. (1992) in *Advances in Inorganic Chemistry* (Cammack, R., Ed.) Vol. 38, pp 281−322, Academic Press, San Diego, CA.

Cammack, R., Dickson, D., & Johnson, C. (1977) in *Iron Sulfur Proteins* (Lovenberg, W., Ed.) Vol. III, pp 283−330, Academic Press, New York.

Chae, Y. K., Abildgaard, F., Mooberry, E. S., & Markley, J. L. (1994a) *Biochemistry 33*, 3287−3295.

Chae, Y. K., Xia, B., Cheng, H., Oh, B.-H., Skjeldal, L., Westler, W. M., & Markley, S. W. (1994b) in *NMR of Paramagnetic Macromolecules* (La Mar, G. N., Ed.), Kluwer Publishers, Amsterdam, The Netherlands.

Conover, R. C., Kowal, A. T., Fu, W., Park, J.-B., Aono, S., Adams, M. W. W., & Johnson, M. K. (1990) *J. Biol. Chem. 265*, 4562−4564.

Donaire, A., Gorst, C. M., Zhou, Z.-H., Adams, M. W. W., & La Mar, G. N. (1994) *J. Am. Chem. Soc. 116*, 6841−6849.

Dugad, L. B., La Mar, G. N., Banci, L., & Bertini, I. (1990) *Biochemistry 29*, 2263−2271.

Dunham, W. R., Palmer, G., Sands, R. H., & Bearden, R. J. (1971) *Biochim. Biophys. Acta 253*, 373−384.

Fiala, G., & Stetter, K. D. (1986) *Arch. Microbiol. 145*, 156−161.

Fukuyama, K., Nagahara, Y., Tsukihara, T., Katsube, Y., Hase, T., & Matsubara, H. (1988) *J. Mol. Biol. 199*, 183−193.

Gaillard, J., Albrand, J.-P., Moulis, J.-M., & Wemmer, D. E. (1992) *Biochemistry 31*, 5632−5639.

Gaillard, J., Moulis, J.-M., Kümmerle, R., & Meyer, J. (1993) *Magn. Reson. Chem. 31*, S27−S30.

Holm, R. H., Ibers, J. A. (1977) in *Iron Sulfur Proteins*, (Lovenberg, W., Ed.) Vol. III, pp 206−281, Academic Press, New York.

Howard, J. B., & Rees, D. C. (1991) *Adv. Protein Chem. 42*, 199−281.

Inubushi, T., & Becker, G. D. (1983) *J. Magn. Reson. 51*, 128−133.

Jeener, B. H., Meier, P., Bachmann, P., & Ernst, R. R. (1975) *J. Chem. Phys. 71*, 4546−4553.

Kissinger, C. R., Sieker, L. C., Adman, E. T., & Jensen, L. H. (1991) *J. Mol. Biol. 219*, 693−715.

La Mar, G. N., & de Ropp, J. S. (1993) in *Biological Magnetic Resonance* (Berliner, L. J., & Reuben, J., Eds.) Vol. 12, pp 1−78, Plenum Press, New York.

Langen, R., Jensen, G., Jacob, U., Stephens, P. J., & Warshel, A. (1992) *J. Biol. Chem. 267*, 25625−25627.

Luchinat, C., & Ciurli, S. (1993) in *Biological Magnetic Resonance* (Berliner, L. J., & Ruben, J., Eds.) pp 357−420, Plenum Press, New York.

Macedo, A. L., Moura, I., Moura, J., LeGall, J., & Huynh, B. H. (1993a) *Inorg. Chem. 32*, 1101−1105.

Macedo, A. L., Palma, P. N., Moura, I., LeGall, J., Wray, V., & Moura, J. G. (1993b) *Magn. Reson. Chem. 31*, S59−S67.

Münck, E., Papaefthymiou, V., Surerus, K. K., & Girerd, J.-J. (1988) in *Metal Clusters in Proteins* (Que, L., Ed.) ACS Symposium Series, pp 302−325, American Chemical Society, Washington, D.C.

Nettesheim, D. G., Harder, S. R., Feinberg, B. A., & Otvos, J. D. (1992) *Biochemistry 31*, 1234−1244.

Neuhaus, D., & Williamson, M. (1989) *The Nuclear Overhauser Effect in Structural and Conformational Analysis*, VCH Publications, New York.

Neuner, A., Jannasch, H. W., Belkin, S., & Stetter, K. O. (1990) *Arch. Microbiol. 153*, 205−207.

Oh, B.-H., & Markley, J. L. (1990) *Biochemistry 29*, 3993−4004, 4012−4017.

Phillips, W. D., & Poe, M. (1973) in *Iron Sulfur Proteins* (Lovenberg, W., Ed.) Vol. II, pp 255−285, Academic Press, New York.

Skjeldal, L., Westler, W. M., Oh, B.-H., Krazel, A. M., Holden, H. M., Jacobsen, B. L., Rayment, I., & Markely, J. L. (1991) *Biochemistry 30*, 7363−7368.

Stout, C. D. (1989) *J. Biol. Chem. 263*, 9256−9266.

Teng, Q., Zhou, Z. H., Smith, E. T., Busse, S. C., Howard, J. B., Adams, M. W. W., & La Mar, G. N. (1994) *Biochemistry 33*, 6316−6326.

Thompson, A. J. (1985) in *Metalloproteins* (Hanson, P., Ed.) Part I, pp 79−120, Verlag Chemie, Weinheim, FRG.

Wüthrich, K. (1986) *NMR of Proteins and Nucleic Acids*, John Wiley & Sons, New York.

Ye, X. M., Pochapsky, T. C., & Pochapsky, S. S. (1992) *Biochemistry 31*, 1961−1968.